Weather and Climate Extremes 40 (2023) 100556

Contents lists available at ScienceDirect

Weather and Climate Extremes

journal homepage: www.elsevier.com/locate/wace

Extreme rainfall events in Morocco: Spatial dependence and climate drivers

Abdelaziz Chaqdid [a,b,*], Alexandre Tuel [c], Abdelouahad El Fatimy [a], Nabil El Moçayd [a,d]

[a] Institute of Applied Physics, Mohammed VI Polytechnic University, Ben Guerir, Morocco
[b] Centre de Recherche Systemes Complexes et Interactions, Centrale Casablanca, Casablanca, Morocco
[c] Institute of Geography and Oeschger Centre for Climate Change Research, University of Bern, Bern, Switzerland
[d] International Water Research Institute, Mohammed VI Polytechnic University, Ben Guerir, Morocco

ARTICLE INFO

Dataset link: https://doi.org/10.24381/cds.adbb2d47, https://www.cpc.ncep.noaa.gov/products/precip/CWlink/daily_ao_index/history/history.shtml, https://www.psl.noaa.gov/mjo/mjoindex/

Keywords:
Extreme precipitation
Extremal dependence
Regional clustering
Climate drivers
Morocco

ABSTRACT

The history of Morocco is replete with tragic natural disasters related to floods that led to numerous casualties and significant material losses. An important driver of these floods is extreme precipitation. Understanding the spatial characteristics of extreme precipitation events is critical to accurately predicting, assessing, and mitigating the risks they pose. Yet, the physical drivers of extreme precipitation events (EPEs) in Morocco remain poorly known. To address this gap, we apply a clustering method to divide Morocco into regions that are spatially consistent in terms of extreme precipitation. We then determine the drivers of extreme precipitation by analyzing atmospheric circulation anomalies during the occurrence of some well chosen EPEs in each region. Our findings suggest that Morocco can be subdivided into 5 spatially coherent regions. Extreme precipitation in the northwestern regions is associated with patterns similar to the negative phase of the North Atlantic Oscillation (NAO) with strong upper-level flow anomalies enhanced by Greenland blocking and/or Rossby wave breaking (RWB) episodes. By contrast, the southern regions are associated with relatively weak upper air troughs but strong water vapor transport anomalies from the tropics.

1. Introduction

It is by now well-documented that extreme precipitation events (EPEs) have generally increased in frequency and intensity due to anthropogenic global warming, and will continue to do so in the future (Westra et al., 2013; IPCC, 2012, 2022). Therefore, assessing and mitigating the risks posed by EPEs is becoming increasingly critical worldwide. However, poor countries are often the least prepared for this, especially in terms of the necessary infrastructure. Most African countries are highly vulnerable to EPEs already in the present climate, a vulnerability which may even be exacerbated in the future due to climate change impacts but also to intensive urbanization (Douglas et al., 2008). For example, the increasing demand for housing as population grows may lead to housing development in floodplains; and urban sprawl results in less permeable soils and thus higher runoff coefficients (Douglas et al., 2008; Arnone et al., 2018). Morocco in particular has already demonstrated how vulnerable it was to floods triggered by extreme precipitation (Satour et al., 2021). Indeed, between 1951 and 2015, more than 35 major floods were reported in the country (Aide et al., 2015), which caused considerable material and human losses (the flash floods in Guelmim (Theilen-Willige et al., 2015), Ouarzazate (Fink and Knippertz, 2003), and the Ourika valley (Saidi et al., 2010), for instance).

Many previous studies have focused on various aspects of monthly- or seasonal-mean precipitation in Morocco, such as its relationship with weather regimes (Knippertz et al., 2003; Gadouali et al., 2020), its inter-annual variability and trends (Ward et al., 1999; Driouech et al., 2021), seasonal forecasting (El Hamly and Sebbari, 1998; Tuel and Eltahir, 2018), and future projections (Filahi et al., 2017; Tuel et al., 2021; Balhane et al., 2022). Several studies have also looked at extreme precipitation in Morocco, specifically its past and future trends, and associated weather/climate features. Past trends were investigated by Tramblay et al. (2012), Filahi et al. (2016), Khomsi et al. (2016) and Benabdelouahab et al. (2020) who found no significant trends in observations except for a few stations in northern and central Morocco. These findings are based on daily precipitation data, but several other studies have indicated the possibility of substantial changes in sub-daily precipitation extremes. This may explain why the impact of climate change on extreme precipitation has not been detected in the aforementioned studies. On the other hand, future scenarios using either global climate model (GCM) or regional climate model (RCM) simulations indicate that extreme precipitation percentiles are very likely to decrease by the end of the twenty-first century over Morocco (Tramblay et al., 2012; Tramblay and Somot, 2018). However, due to large uncertainties, the reliability of these simulations remains

* Corresponding author at: Institute of Applied Physics, Mohammed VI Polytechnic University, Ben Guerir, Morocco.
E-mail address: Abdelaziz.Chaqdid@um6p.ma (A. Chaqdid).

https://doi.org/10.1016/j.wace.2023.100556
Received 28 November 2022; Received in revised form 9 March 2023; Accepted 10 March 2023
Available online 16 March 2023

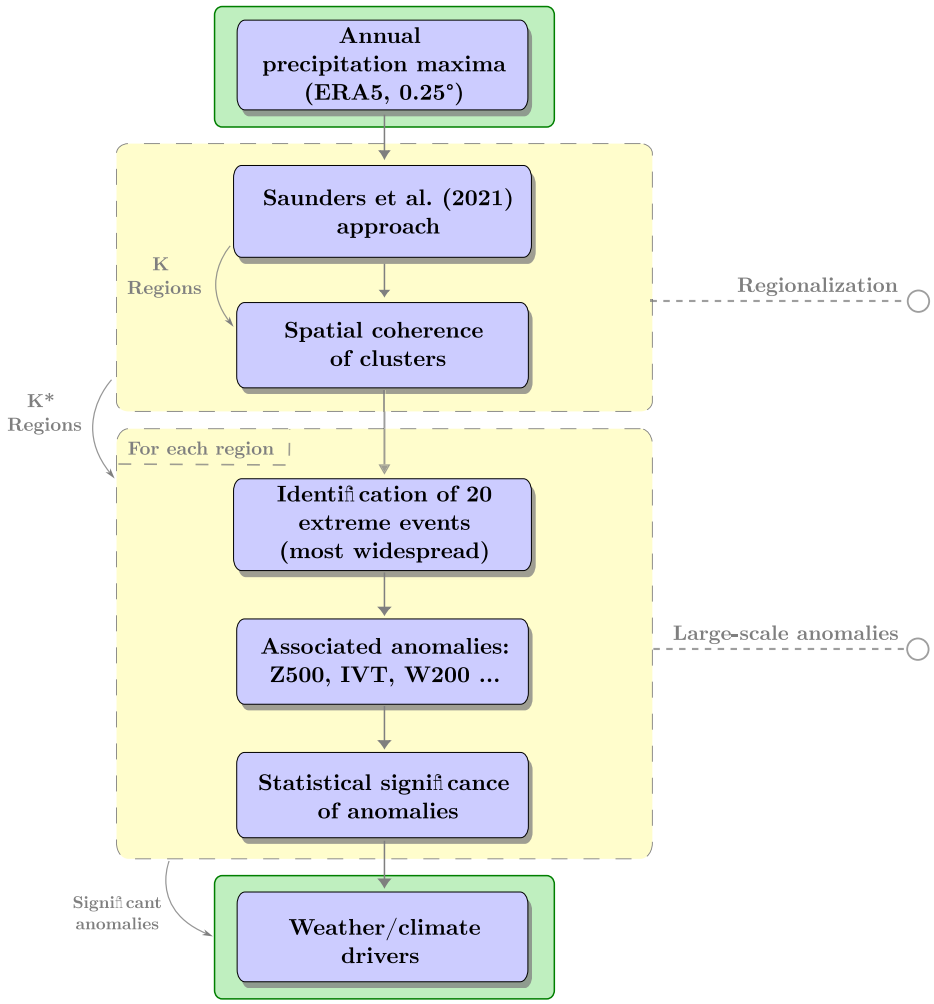

Fig. 1. Flow chart of data and methodology.

questionable for different reasons. First, models still poorly simulate extreme precipitation in complex terrain that makes up a significant fraction of Moroccan territory (Tuel, 2020). Additionally, numerical simulations exhibit high variability in space and time (Tramblay et al., 2012; Filahi et al., 2017).

Based on past studies, most of the variability in Moroccan winter precipitation can be attributed to the North Atlantic Oscillation (NAO) (Lamb and Peppler, 1987; El Hamly and Sebbari, 1998; Knippertz et al., 2003). Extreme precipitation, by contrast, is characterized by high spatio-temporal variability. As a result, it is only moderately correlated to modes of large-scale circulation (Tramblay et al., 2013). Still, several studies have been able to identify connections between canonical modes of large-scale circulation variability and heavy precipitation in Morocco. In the northern half the country, the NAO, the Mediterranean Oscillation (MO) and North Atlantic Blocking (NABl) seem to play a role by modulating the location of the stormtrack (Tramblay et al., 2012; Gadouali et al., 2020). By contrast, extreme precipitation in southern Morocco has been linked to tropical–extratropical interactions through synoptic features, such as tropical moisture plumes (also known as atmospheric rivers) (Fink and Knippertz, 2003; Knippertz and Martin, 2005; Khouakhi et al., 2022), potentially influenced by the Madden–Julian Oscillation (MJO) (Schreck III, 2021).

Climate drivers of extreme precipitation thus strongly differ from one region to another. Extreme precipitation may also respond differently to climate change across Morocco. Future trends were indeed found to vary substantially between southern and northern Morocco (Khomsi et al., 2016) and between the Atlantic and Mediterranean coastlines (Tramblay et al., 2012; Filahi et al., 2017).

A first step to address risks and better understand climate change impact on EPEs and evaluate the reliability of climate simulations regarding future trends is to assess the spatial distribution and drivers of EPEs in Morocco. To this end, we introduce a regionalization procedure that partitions Morocco into several spatially homogeneous regions with similar timing of extreme precipitation (Fig. 1). We then analyze the synoptic-scale anomalies associated with EPEs in each region. This analysis allows to identify the main climatic drivers at synoptic scale responsible for the occurrence of extreme precipitation in each region.

Accordingly, this paper will be organized as follows. In Section 2, we present the data and methods used in this study, followed by the regionalization results in Section 3 and the analysis of synoptic-scale anomalies in Section 4. We end by summarizing our main findings and discussing some potential applications and future perspectives.

2. Data and methods

2.1. Data

This study relies on data from the ECMWF ERA5 reanalysis (Hersbach et al., 2020). We consider the following variables, for the 1979–2020 period, at a daily resolution: precipitation with a spatial resolution of 0.25° × 0.25°; sea surface temperature (SST), geopotential height at 500 hPa (Z500), wind speed at 200 hPa (W200), total column water (TCW), integrated water vapor transport (IVT) between 1000 and 100 hPa, and daily Ertel potential vorticity (PV) at the 320 K isentropic level, all at a 1° × 1° spatial resolution. PV is interpolated to

the 320 K isentropic level using ERA5 model-level wind, temperature, and pressure. We also use daily binary block and cyclone detection indices over the time period 1979–2020, at 1° x1° spatial resolution, calculated by Rohrer et al. (2020). We investigate the physical drivers of EPEs in light of the three key ingredients of extreme precipitation: moisture availability, ascent, and persistence over time (Doswell et al., 1996). IVT and TCW are related to moisture availability, while Z500, W200, cyclone and blocking frequency and PV relate to persistence in large-scale dynamics and ascent. We also consider the daily MJO (OLR-based) OMI index (Kiladis et al., 2014) and the daily NAO index, both obtained from the National Centers for Environmental Prediction.

The choice of ERA5 data over observations is motivated by the fact that ground stations are unevenly distributed across the study area, with a high density to the north and a very low density, if any, to the south (Tuel, 2020). By contrast, reanalysis data comes on a regular grid which allows a more robust implementation of clustering algorithms. While precipitation is not assimilated in ERA5, Rivoire et al. (2021) found that extreme and moderate precipitation in ERA5 agreed well with satellite estimates over midlatitude regions, as well as with observational data in regions with enough input stations. Furthermore, a separate analysis of extreme precipitation indices in Morocco conducted by Tuel and Moçayd (2023), using extensive station data and nine daily gridded precipitation datasets (reanalyses, observation- and satellite-based), found that ERA5 performed well.

2.2. Methods

Our methodology consists of three main steps (Fig. 1). First, we implement a regionalization algorithm to partition Morocco into regions (Section 2.2.1). Then, we check the spatial coherence of the obtained regions (Section 2.2.2). Finally, we define EPEs for each region and compute concurrent circulation anomalies and their significance (Section 2.2.3).

2.2.1. Spatial clustering

Our regionalization is based on the approach originally introduced by Bernard et al. (2013). The latter applied the Partitioning Around Medoids (PAM) algorithm (Leonard and Peter, 1990) to weekly precipitation maxima in France, with the F-madogram distance (Cooley et al., 2006) as a dependence measure. In PAM, cluster centroids are chosen among the observed data points (Leonard and Peter, 1990). This makes PAM better suited to non-Gaussian data (like extreme precipitation) than other algorithms like k-means. The F-madogram was developed specifically to measure the pairwise dependence between block maxima of two station time series. The approach of Bernard et al. (2013) was taken up by other studies to develop more robust approaches that deal with the problem of clustering extreme values. Bracken et al. (2015) modified the F-madogram to take into account the geographic distance between stations to obtain more compact clusters in large geographic regions. Saunders et al. (2021) also used the F-madogram as the distance between station time series, but replaced PAM with hierarchical clustering (HC). PAM may indeed generate false clusters when applied with the F-madogram distance metric (Saunders et al., 2021), while HC is more flexible with the number of clusters determined by the strength of dependency chosen by the user. Considering these advantages, we apply the approach proposed by Saunders et al. (2021); this modified version of Bernard et al. (2013) approach is applied to the annual maxima of daily precipitation in Morocco, calculated on hydrological (September–August) and not calendar years.

2.2.2. Spatial coherence of clusters

The challenge in any clustering approach is to select a satisfactory number of clusters. To do so, we implement a simple evaluation procedure that tests the physical consistency of the resulting clusters. Similar to the well-known hit rate statistic (Rhodes et al., 2015), our procedure is based on the probability of joint occurrence of extreme precipitation inside and outside each cluster (Algorithm B.1). The clustering itself groups together grid points with similar distributions of extreme precipitation. The purpose of the test is to check that the timing of EPEs is consistent between grid points in the same cluster, whereas it varies between grid points from different clusters.

For a given cluster C, let $e_{hit}(i,j)$ be the number of times an extreme event has jointly occurred, within a given time window, in a grid point i belonging to C and in another grid point j (belonging to any cluster). The co-occurrence probability (CoP) in (i,j) is then defined as:

$$CoP(i,j) = \frac{e_{hit}(i,j)}{e_{total}(i)}, \tag{1}$$

where $e_{total}(i)$ is the total number of extreme events recorded in grid point i. In our case, the threshold to separate extreme from non-extreme precipitation days is the 99th percentile of wet days (> 1 mm/day). We also select a time window of one week to calculate CoP. This corresponds approximately to the average lifetime of a synoptic weather system and allows some flexibility in characterizing the simultaneity of extreme precipitation events across space.

We then average $CoP(i,j)$ over all grid points i in C to obtain the average co-occurrence probability of extreme precipitation between grid point j and cluster C:

$$CoP_C(j) = \frac{1}{N-1}\sum_i CoP(i,j), \tag{2}$$

where N is the total number of grid points in C.

2.2.3. Significance of anomalies

Applying the spatial coherence test to the K clusters obtained by the regionalization step yields K*(≤ K) consistent clusters. For each of these clusters, we first identify the twenty 3-day periods during which the most grid points within the cluster experienced extreme precipitation (the threshold for extreme precipitation being the 99th percentile of 3-day totals). Next, we calculate for each of the twenty events the anomalies of the various atmospheric fields introduced in Section 2.1, by subtracting the climatological average from the mean variable field during the 3-day event. Finally, we calculate the mean anomaly of each variable by averaging over the 20 events. The statistical significance of the obtained anomalies is determined by bootstrapping (Algorithm B.2). We calculate a p-value at each grid point based on the rank of the anomaly within 2000 randomly generated anomaly fields. This p-value is derived from Weibull's formula for plotting position (Weibull, 1939), using a symmetric rank such that positive anomalies (higher rank) and negative anomalies (lower rank) have the lowest p-value:

$$Pr(i) = \frac{2\left(\frac{N}{2} - \left|i - \frac{N}{2} + 1\right|\right)}{N+1}, \tag{3}$$

where i is the rank of the anomaly and N is the sample size. The resulting $p\text{-}values$ are then adjusted using the false discovery rate (FDR) method (Wilks, 2016).

2.2.4. Seasonal frequency analysis of extratropical cyclones

Studies have demonstrated the relevance of extratropical cyclones in the transport of moisture to mid-latitude regions, and the role of the Warm Conveyor Belts (WCBs) within these cyclones in triggering EPEs in the extratropics (Browning, 1986; Pfahl and Wernli, 2012; Binder et al., 2016). In addition to maps of cyclone frequency anomaly, we analyze the direction from which cyclones associated with EPEs in each region came. To that end, for each of the K* regions, we identify the individual cyclones that affected the region during the corresponding EPEs, and then trace each cyclone back in time to identify its position 7 days before the EPE. Once the initial positions of the cyclones are identified, we calculate the direction, relative to the center of the region, from which the cyclone originated. Finally, we represent the results as seasonal frequencies on a wind rose plot.

3. Spatial clustering

Having no a priori idea for the optimal number of clusters, we begin by implementing the hierarchical clustering for a cluster number ranging from 2 to 10. At 6 clusters, we obtain the main known climate zones in Morocco (i.e. the Mediterranean to the north, the Sahara desert to the south, the Atlantic Ocean to the west, and the Atlas mountain ranges). Adding more clusters does not lead to a better regionalization: new clusters are not associated with significantly different circulation anomalies than their larger parents, and generally fail the spatial consistency test (not shown). Therefore, we select a cluster number equal to 6. With this number, the Sahara region (southern half of Morocco) is split into two clusters (5 and 6). This is not particularly physically meaningful, and these two separate clusters do not pass the spatial consistency test. Fig. A.1 shows that the co-occurrence probability values are relatively very high outside the boundaries for cluster 6, thus this cluster is not well defined. We expect the probability of co-occurrence of EPEs to tend toward zero far from the cluster boundaries. In other words, only grid points in the cluster should be affected by the same type of EPEs. This problem is likely due to the arid nature of the climate in southern Morocco: the clustering method uses the F-madogram distance whose assumptions are generally not satisfied in dry regions (Saunders et al., 2021). We therefore group the two Saharan clusters, and then check the validity of the five remaining clusters with our spatial coherence test. Results show that the 5-cluster set is spatially coherent (Fig. A.2). Fig. 2 shows the final results of the regionalization approach:

Region 1: the northern cluster, containing the Loukkos and Sebou river basins;

Region 2: the eastern cluster, formed by the Moulouya basin;

Region 3: the Atlantic cluster, containing multiple basins (Bou Regreg, Oum Er-Rbia, Tensift, and Souss Massa);

Region 4: the south-eastern cluster, formed by the South Atlas basin (Guir-Ziz-Rheris);

Region 5: the southern cluster, formed by the Sahara basin (Sakia El Hamra and Oued Eddahab).

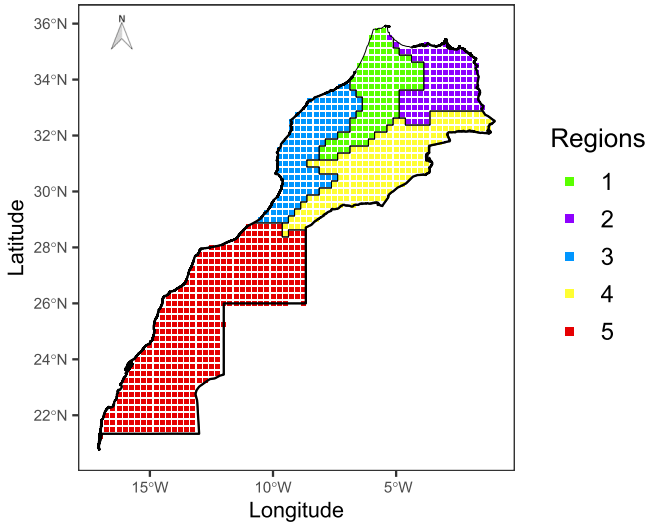

Fig. 2. Regionalization results for Morocco.

Table 1 depicts the seasonal distribution of EPEs in various regions, revealing a prominence of EPEs during the autumn months in Morocco. The analysis shows that the southern regions (Regions 4 and 5) exhibit a concentration of EPEs in autumn, while the northern regions (Regions 1 and 3) experience a higher frequency of EPEs during both autumn and winter.

Table 1
Seasonal frequency (%) of EPEs in each region.

	DJF	MAM	JJA	SON
Region 1	55	0	0	45
Region 2	25	25	10	40
Region 3	40	15	0	45
Region 4	15	20	10	55
Region 5	25	10	5	60

4. Analysis of large-scale conditions during EPEs

4.1. Results

4.1.1. Region 1

Extreme precipitation in Region 1 is associated with a strong trough centered over the Iberian Peninsula and extending into northern Morocco (Fig. 3a). Wind anomalies aloft indicate a stronger and equatorward-shifted jet around 35°N (Fig. 3d), with evidence of anticyclonic Rossby wave breaking (RWB) over the Iberian Peninsula (Fig. A.3a). Moisture availability is provided by a significantly enhanced IVT from the Atlantic towards northern Morocco (Fig. 3b), leading to larger total column moisture in Region 1 (Fig. 3c). Low-level convergence and orographic uplift over the Rif mountains provide the necessary uplift to trigger extreme precipitation in the region. The atmospheric circulation during EPEs in this region is similar to the negative NAO phase. We indeed find a statistically significant negative NAO index during the week prior to EPEs in Region 1 (see Fig. A.4). Furthermore, the results of the seasonal frequency analysis of cyclones (Fig. 8) show that cyclones hitting Region 1 mostly originate over the North Atlantic, particularly in winter when they come directly from the northwest.

4.1.2. Region 2

Large-scale circulation anomalies during EPEs in Region 2 are very different from those found for region 1. Z500 anomalies point to a more intense Azores High, which extends to reach the coasts of the UK and blocks all westerly circulation (Figs. 9 and 4a), in keeping with the positive and statistically significant NAO index detected in the two weeks prior to EPEs in this region (Fig. A.4). This synoptic configuration sets the stage for more tropical–extratropical interactions. Indeed, the seasonal frequency analysis of cyclones (Fig. 8) reveals that Region 2 is frequently affected by winter and summer cyclones generated to the east of the Atlantic Ridge and entering the region from the north-east, as well as autumn and spring cyclones arriving from the south (Tropics). Furthermore, we examined the Madden–Julian oscillation (MJO) index and found that Region 2 may be further enhanced by the MJO's phases 2–3 (Fig. A.5), in consistency with the well known role of these phases in triggering the positive NAO (Cassou, 2008).

4.1.3. Region 3

Weather patterns during EPEs over Region 3 are similar to those of Region 1, but generally more pronounced (Fig. 5). Enhanced cyclone frequency over southwestern Europe is associated with a pronounced trough and enhanced westerly and northwesterly IVT into Morocco. The jet streak above Morocco is noticeably stronger than in the case of Region 1 (Fig. 3d). The shape of the dynamical tropopause indicates strong anticyclonic RWB with a pronounced stratospheric PV streamer stretching southwards into Morocco (see Fig. A.3c). An important difference with region 1, however, is the presence of significant blocking anomalies southwest of Greenland (Newfoundland) (Fig. 5e). Quasi-geostrophic lifting in the cyclones' WCBs, enhanced by orographic lifting as the air flow hits the Atlas Range, provide the necessary ascent to trigger extreme precipitation. Furthermore, EPEs in this region are also preceded by a negative NAO phase persisting for a whole week

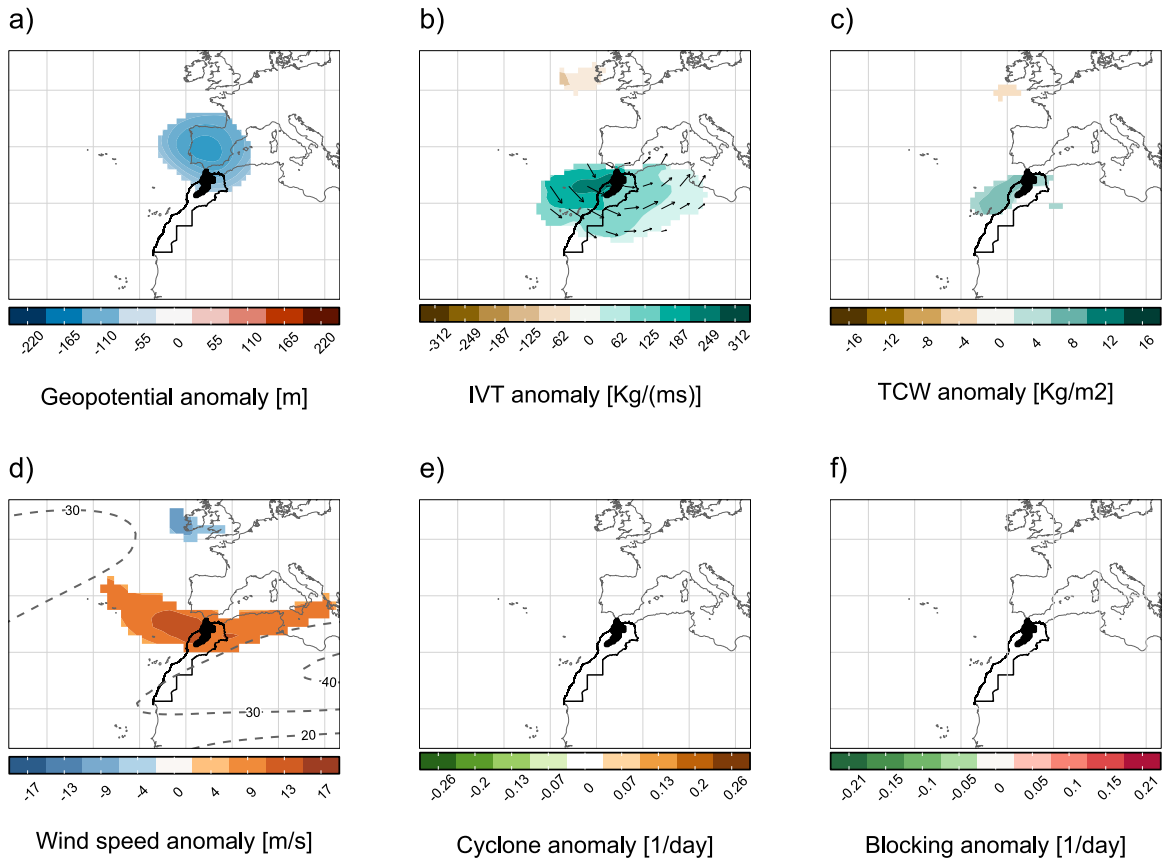

Fig. 3. Average anomalies of large-scale conditions associated with EPEs in Region 1; (a) Geopotential heights at 500 mb, (b) Vertical integral of water vapor flux, (c) Total column water, (d) Wind speed at 200 mb (shaded) against the climatological mean represented in dashed contours, (e) Cyclone frequency, and (f) Blocking frequency. Only significant anomalies, according to *Algorithm B.2*, are displayed. Black color is used to highlight the geographical extension of the cluster.

prior to EPEs (Fig. A.4). Although the literature suggests that phases 5–6 of the MJO are traditionally precursors to the negative NAO phase in mid-latitudes (Cassou, 2008; Gadouali et al., 2020), this is not found in our case. Specifically, no statistically significant MJO signal is found preceding the EPEs in both Region 1 and Region 3 (Fig. A.5).

4.1.4. Region 4

The synoptic scale situation for Region 4 is characterized by a trough centered on the western Moroccan coastline around 30°N which extends over the entire southern Atlantic coast (Fig. 6a). Z500 anomalies are consistent with an increased frequency of cyclonic activity at the coast (Fig. 6e) and enhanced southerly and southwesterly IVT (Fig. 6b). We also find significant positive TCW anomalies over Region 4 and stretching southwards to 15°N (Fig. 6c). The moist inflow from the tropics undergoes quasigeostrophic lifting in WCBs along the eastern margin of the trough. Ascent is further enhanced by orographic uplift on the southern slopes of the High Atlas in region 4. The majority of cyclones affecting Region 4 during autumn originate from the Atlantic Ocean, with a significant proportion also occurring during summer and autumn and originating from the southeast (Fig. 8). Furthermore, the analysis of the MJO index shows that phase 3 of the MJO is a precursor to extreme precipitation in this region (Fig. A.5).

4.1.5. Region 5

Finally, EPEs in Region 5 are connected to a trough west of the region (Fig. 7a), along with increased wind speed aloft on the eastern side of the trough (Fig. 7d). The circulation is associated with significant southerly IVT which brings large positive TCW anomalies throughout region 5 (Fig. 7b). We also find an increase in cyclone frequency along the coast of Region 5 (Fig. 7e). Uplift seems connected to quasi-geostrophic lifting in the WCB of these cyclones. The cyclones that affect region 5 come mainly from two directions: the North Atlantic in autumn and winter and the southeast in autumn (Fig. 8).

4.2. Discussion

EPEs occur when lifting combines with moisture availability to trigger condensation and precipitation. Synoptic conditions during EPEs highlight important differences but also similarities across regions in terms of moisture sources, lifting mechanisms and large-scale dynamics.

4.2.1. Modes of climate variability

The NAO is known to have a major influence on winter atmospheric dynamics and precipitation, including extreme events, in northwestern Africa (Scaife et al., 2008; Tuel and Martius, 2022). There, a significant negative correlation exists between the NAO index and extreme precipitation (Krichak et al., 2014). This is consistent with the finding of a predominantly negative NAO index during EPEs in Regions 1 and 3. Other modes of climate variability could also explain a significant fraction of extreme precipitation variability in Northwestern Africa: the Arctic Oscillation (AO), the Scandinavian Oscillation (SO), the El Niño Southern Oscillation (ENSO) (Krichak et al., 2014), and the MJO (Gadouali et al., 2020; Schreck III, 2021). The physical link between specific MJO phases and extreme precipitation in the extratropics, notably northwestern Africa, remains elusive, especially given that the physical processes underlying the MJO are also not yet fully understood (Jiang et al., 2020). Most studies have therefore examined the effects of the MJO on EPEs from a statistical perspective (e.g., Jones et al., 2004; Schreck III, 2021). We similarly looked at the statistical relationship between the MJO and extreme precipitation

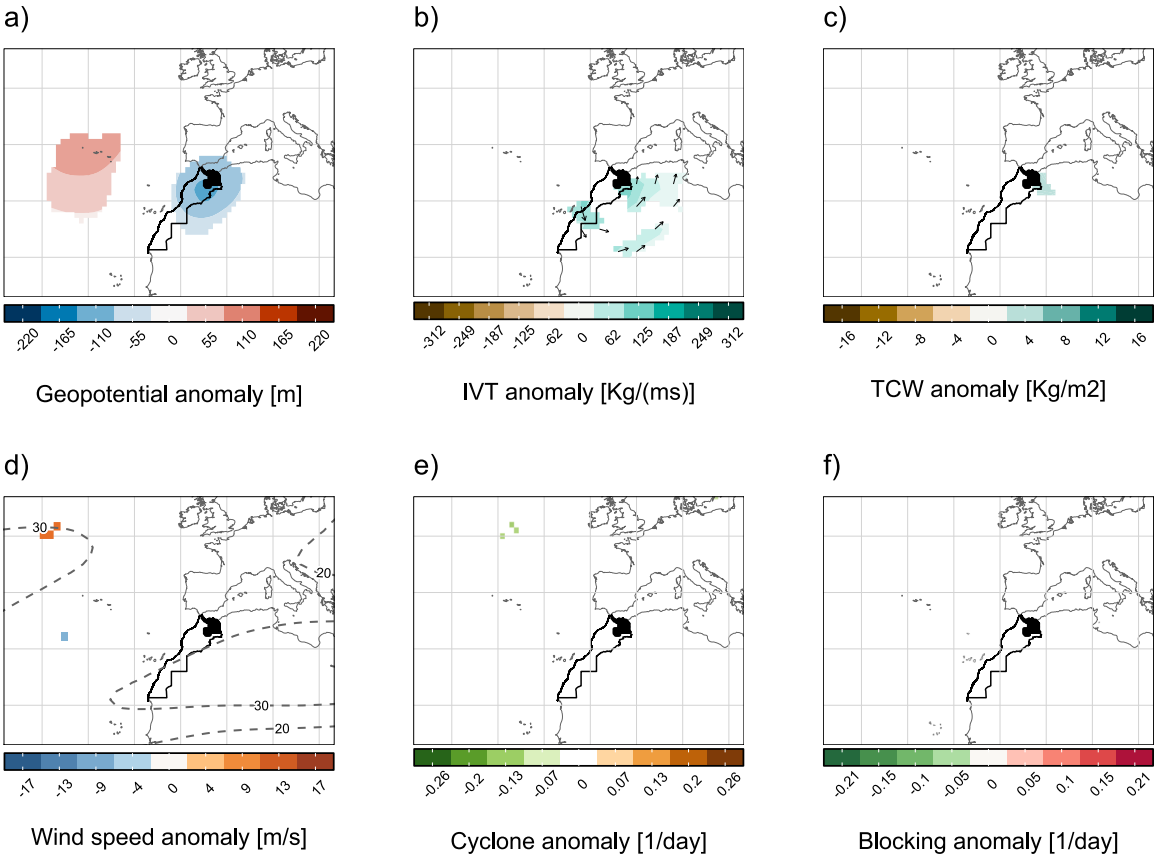

Fig. 4. As in Fig. 3, but for Region 2.

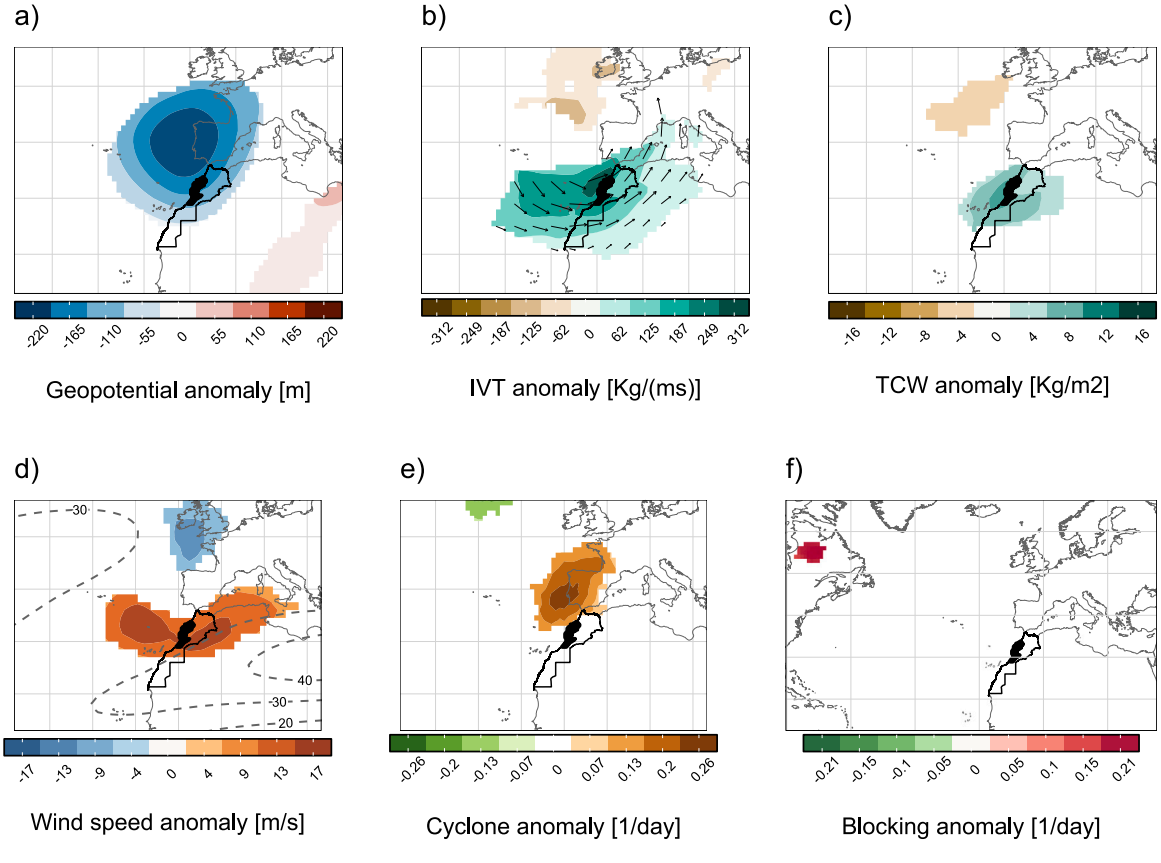

Fig. 5. As in Fig. 3, but for Region 3.

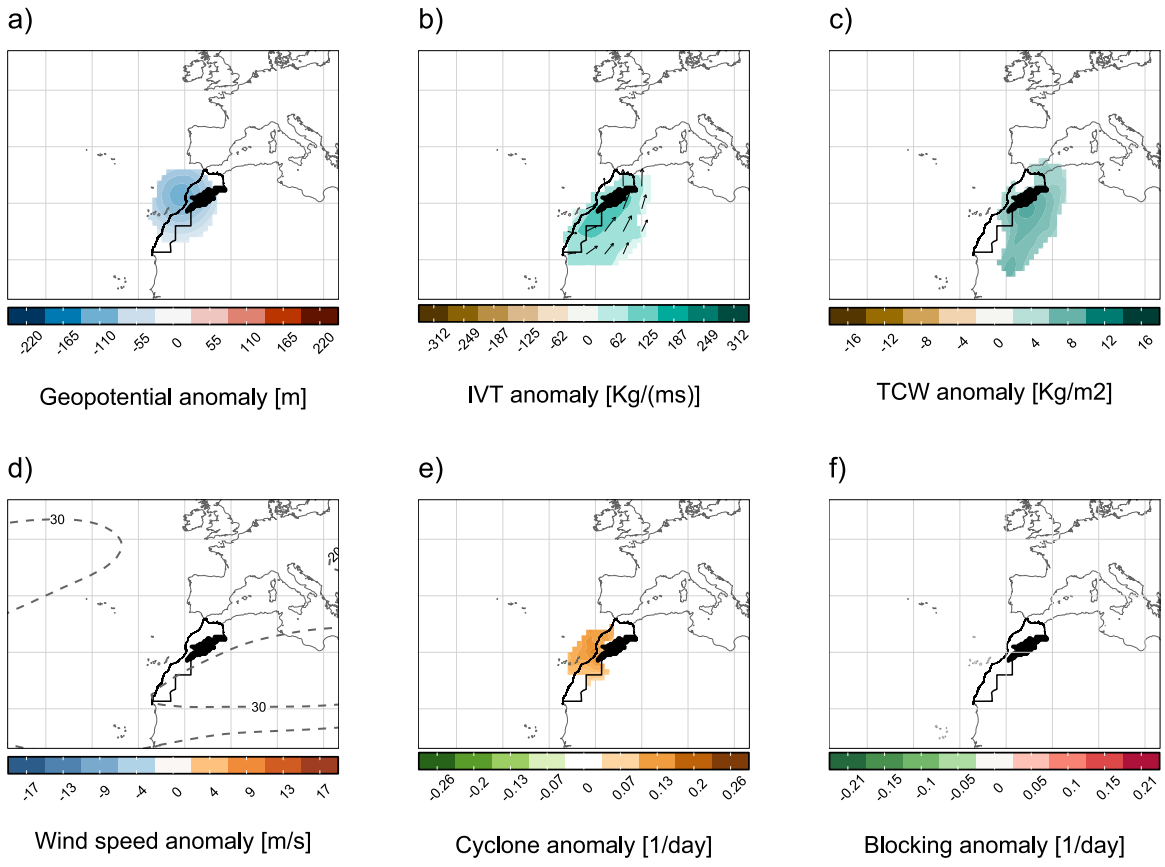

Fig. 6. As in Fig. 3, but for Region 4.

in Morocco, but did not discuss potential causal mechanisms. We found that EPEs in southern and eastern Morocco (regions 2 and 4) were linked to significant MJO anomalies. This is consistent with the fact that these two regions, because of their geography, are less impacted by mid-latitude dynamics over the North Atlantic. They may therefore experience more frequent tropical–extratropical interactions, especially in spring and autumn (Fig. 8) or when the mid-latitude jet is shifted polewards (positive NAO phase; Fig. 4).

4.2.2. Moisture sources

Our findings show that EPEs in the Atlantic regions of Morocco (Region 1 and Region 3) are linked to enhanced westward IVT, which brings moist and mild air masses from the North Atlantic. These results are consistent with the North Atlantic being the primary source of moisture for western Mediterranean land areas (Northwestern Africa, Iberian Peninsula), resulting in 65% of winter and autumn precipitation and 50% of spring and summer precipitation (Batibeniz et al., 2020). On the other hand, EPEs in southern regions (Region 4 and Region 5) are associated with anomalous southerly IVT that brings very moist, warm, and unstable air from the tropics. They are associated with atmospheric rivers or tropical plumes stretching into Morocco (Khouakhi et al., 2022) and lead to large positive TCW anomalies in Regions 4 and 5. Backward trajectory analyses during EPEs in the southern Moroccan and northwest African regions even reveals a significant contribution from continental moisture generated over the Sahel (Fink and Knippertz, 2003; Knippertz and Martin, 2005). This type of intense moisture transport is linked to tropical easterly waves and is often associated with EPEs over North Africa (De Vries, 2021). In contrast to regions 1 and 3, moisture availability in region 2 is not influenced by the westerly circulation since it is blocked by the Rif, High Atlas and Middle Atlas mountain ranges. Moisture availability in this region is mainly ensured by the IVT originating from the North Atlantic and entering Region 2 from the south side after circumventing the Atlas mountain range. In addition, the Azores High strengthens during the EPEs of Region 2, resulting in a meridional flow over Morocco. This situation allows cyclones generated in the Mediterranean to move across Region 2, especially during winter and summer (Fig. 8). A similar weather pattern was identified in Merino et al. (2016); their "cluster 5" is also distinguished by a strong anticyclone over the North Atlantic inducing southward advection of high-latitude air masses towards the Iberian Peninsula.

4.2.3. Ascent

Ascent during EPEs in Morocco is provided by two main mechanisms: first, quasi-geostrophic lifting ahead of troughs; and second, orographic lifting triggered by the numerous mountain ranges in the country. Mountain ranges indeed cover more than a third of the Moroccan territory, reaching high elevations (> 4000 m). Orographic uplift plays an important role chiefly over the northern half of Morocco, where mountains block moisture transport in its path (Lin et al., 2001). Ascent can also result from quasi-geostrophic lifting (or dynamic lifting) associated with troughs and sometimes RWB events (as in Region 1 and Region 3) (De Vries, 2021). Significant cyclone activity is indeed identified in all five regions during EPEs. The WCBs within these extratropical cyclones play an important role in the generation of EPEs over Morocco, especially in the southern region where there is no orographic lifting. These strong upward motions of moisture (WCBs) in the North Atlantic are more frequent in winter and may become even more frequent with higher values of the NAO index (Eckhardt et al., 2004). Stronger WCBs are also associated with more intense extratropical cyclones and result in heavier rainfall (Binder et al., 2016). In Region 2 and Region 4, we also found that EPEs are preceded by phases 3 and 4 of the MJO, suggesting that synoptic perturbations during EPEs in these regions are likely to be strengthened by the MJO. Schreck III (2021) likewise

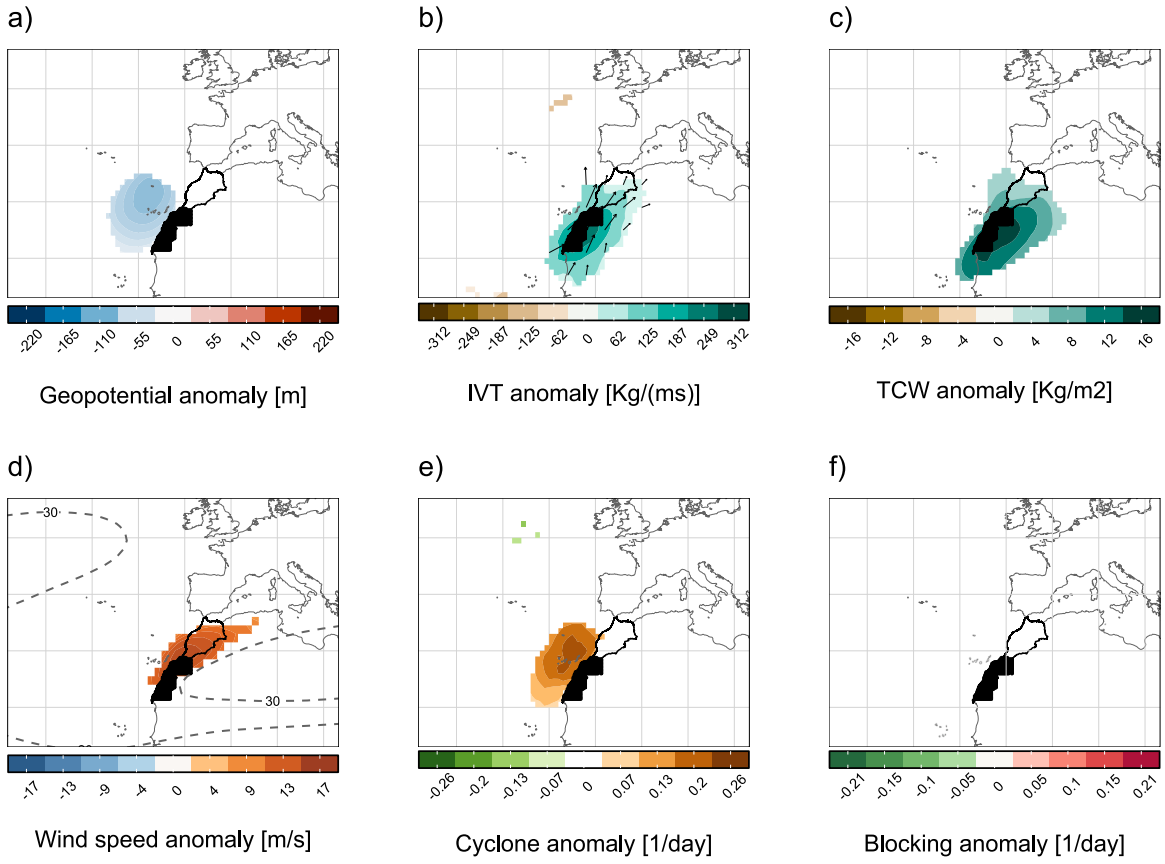

Fig. 7. As in Fig. 3, but for Region 5.

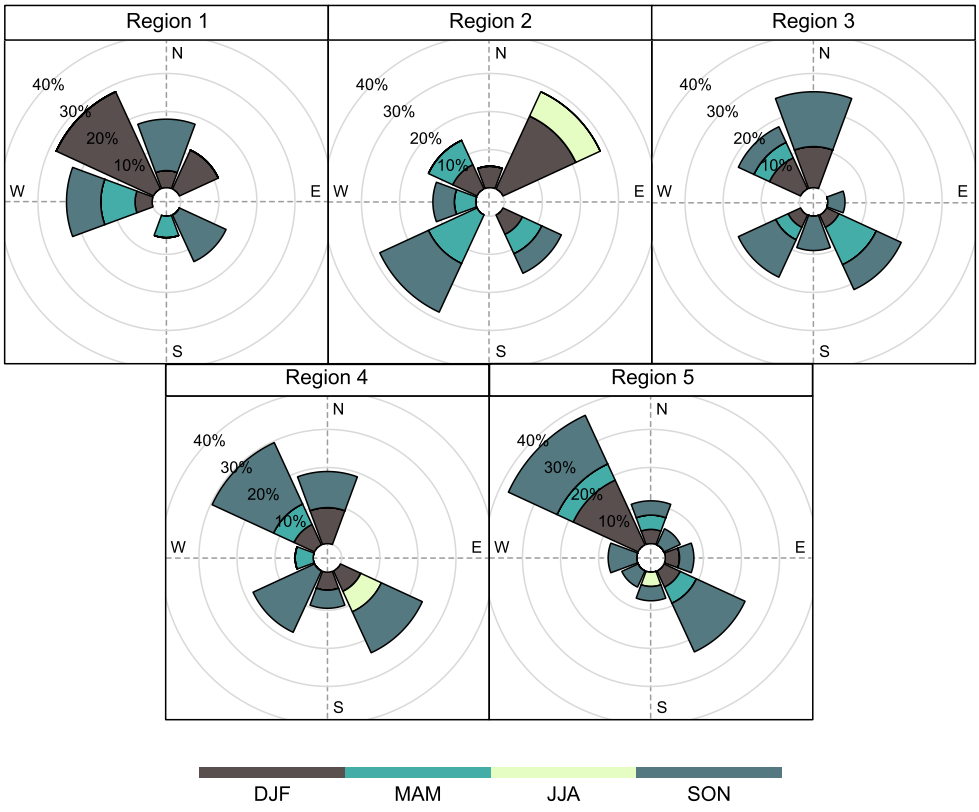

Fig. 8. Seasonal distribution of cyclone origin during EPEs in Morocco (see Section 2.2.4).

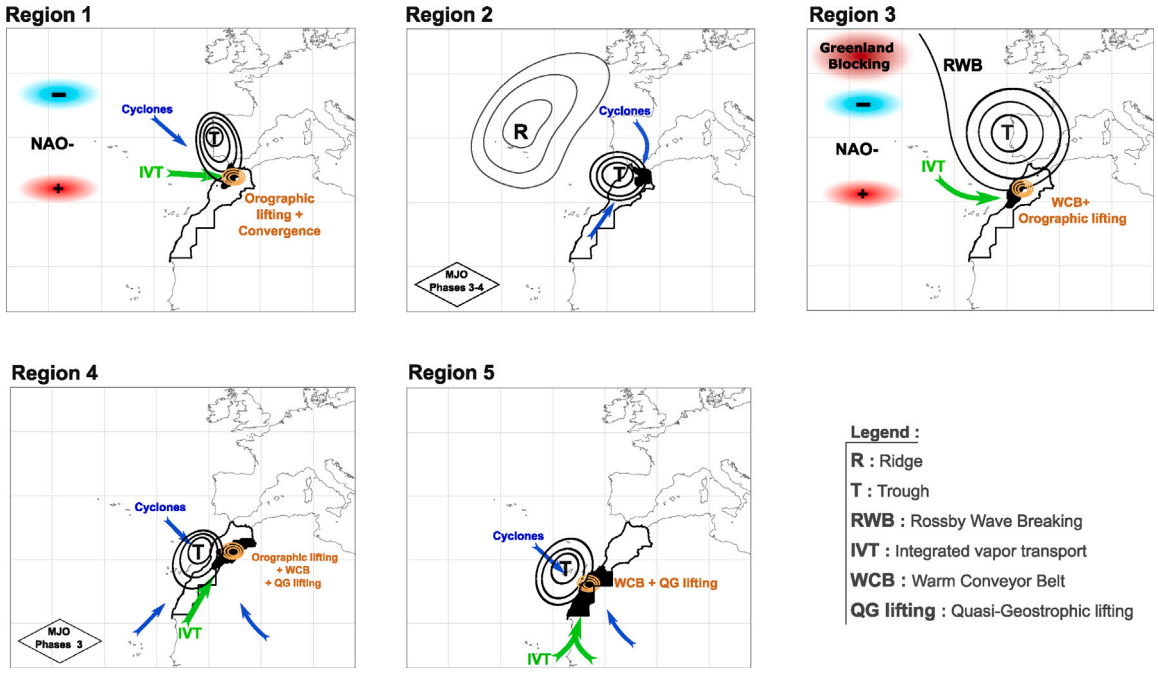

Fig. 9. Climate/Weather factors identified for each of the five regions (Fig. 2).

reported that a significant frequency of co-occurrence of EPEs and MJO phases 2–3 has been identified in Northwest Africa.

5. Conclusions

The aim of this study was to identify the key climate/weather drivers and moisture sources that contribute to the generation of extreme precipitation over Morocco. Knowing that climate varies a lot across Morocco, we used a regionalization approach based on annual precipitation maxima to divide Morocco into 5 spatially coherent regions. By analyzing large-scale atmospheric conditions during EPEs in each region, we were able to identify and describe different climate factors affecting EPEs across Morocco (Fig. 9). In Region 1 and Region 3, EPEs are associated with patterns similar to the negative phase of the NAO with strong upper-level flow anomalies, which are further enhanced by the Greenland blocking and/or Rossby wave breaking (RWB) episodes. By contrast, the large-scale situation in Region 2 is characterized by a pronounced Azores High, which blocks westerly circulations and creates favorable conditions for tropical–extratropical interactions, especially through the MJO. On the other hand, Region 4 and Region 5 exhibit relatively weak upper air troughs, but strong water vapor transport anomalies from the tropics.

Our results can be used either to assess and mitigate the risk of EPEs on the economy and on the lives of citizens, or to be used by hydrologists and other researchers to improve our understanding of the hydrological implication of extreme precipitation in Morocco. Future research may consider implementing the approach used in this study to assess the regionalization and physical drivers of other weather extremes in Morocco, such as cold and heat waves. Furthermore, applying the same approach to precipitation projections can provide a good foundation for assessing the impacts of climate change on EPEs in Morocco. We also suggest that the regionalization results obtained as well as the significance tests performed for atmospheric variables can be exploited as a feature selection step in the development of statistical downscaling models for extreme precipitation forecasts/projections in Morocco.

CRediT authorship contribution statement

Abdelaziz Chaqdid: Data analysis, Formal analysis, Visualization, Writing. **Alexandre Tuel:** Conceptualisation, Methodology, Data collection, Formal analysis, Visualization, Writing. **Abdelouahad El Fatimy:** Writing, Funding acquisition. **Nabil El Moçayd:** Conceptualisation, Methodology, Writing, Funding acquisition.

Declaration of competing interest

The authors declare that they have no known competing financial interests or personal relationships that could have appeared to influence the work reported in this paper.

Data availability

ERA5 reanalysis data are available at https://doi.org/10.24381/cds.adbb2d47. Teleconnection indices are available at: https://www.cpc.ncep.noaa.gov/products/precip/CWlink/daily_ao_index/history/history.shtml(NAO index), and https://www.psl.noaa.gov/mjo/mjoindex/ (MJO index).

Acknowledgments and funding

The authors thank the Fondation Ecole Centrale Casablanca for funding the thesis of A.C. This work was also undertaken in the framework of the UMRP project. The financial support from OCP was highly appreciated. We would also like to thank Reviewers for taking the necessary time and effort to review the manuscript. We sincerely appreciate all the valuable comments and suggestions, which helped considerably in improving the quality of the paper.

Appendix A. Figures

See Figs. A.1–A.5.

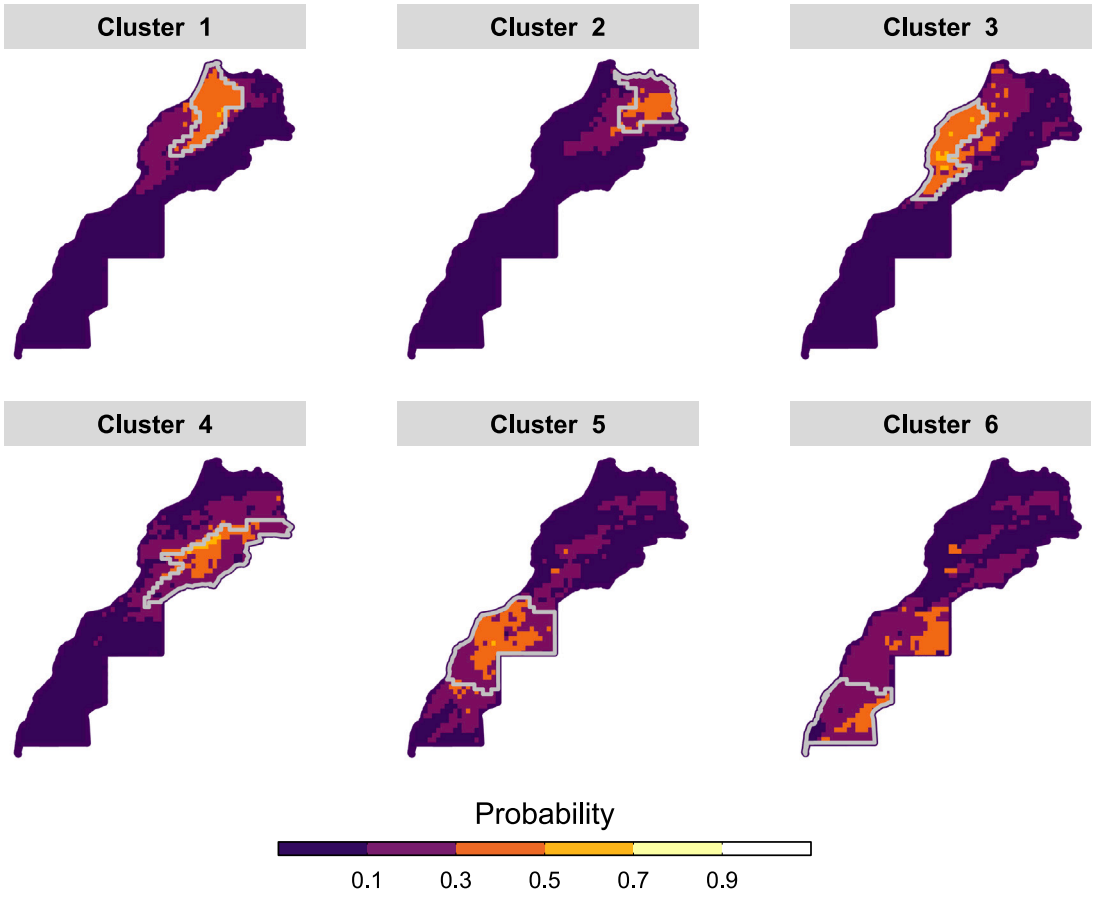

Fig. A.1. Co-occurrence probabilities of EPEs, calculated with respect to the EPEs of each region, using daily precipitation from the ERA5 database and Algorithm B.1. The 6 clusters are obtained using Saunders et al. (2021) approach.

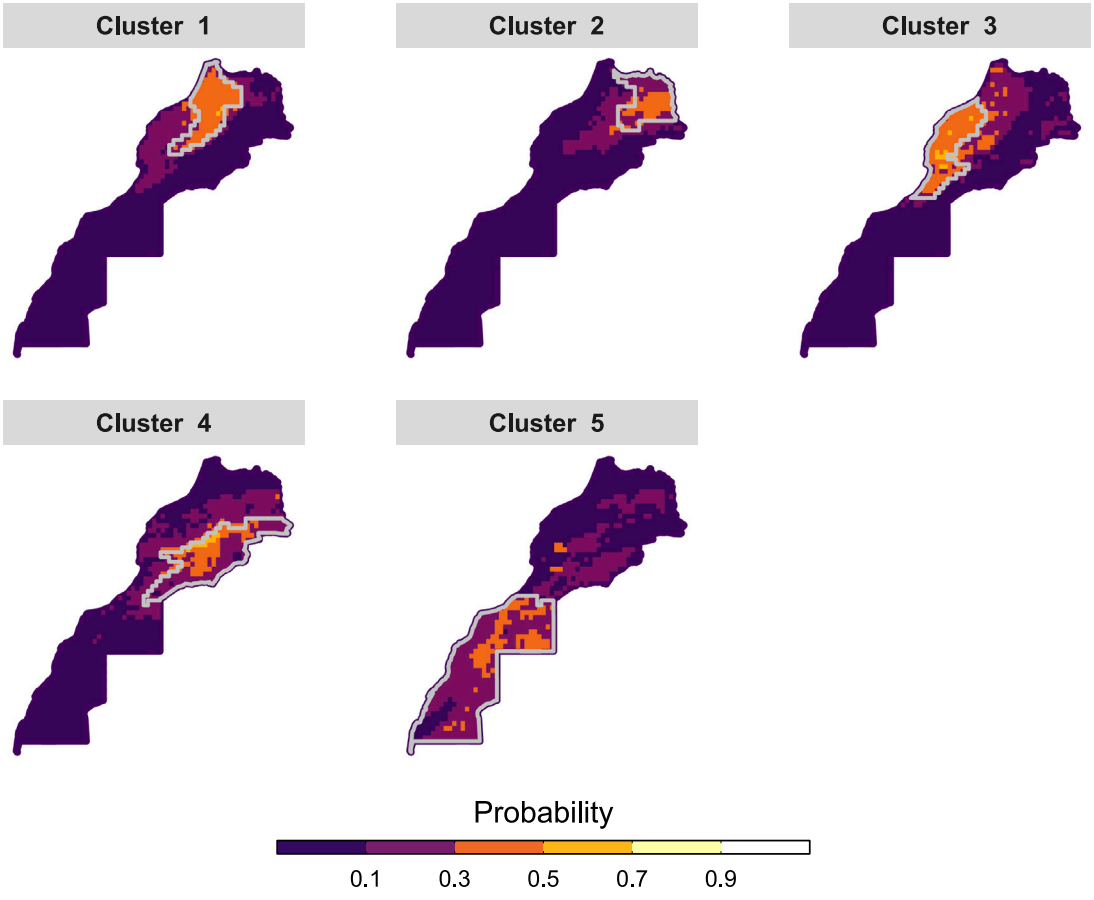

Fig. A.2. As in Fig. A.1, but after grouping clusters 5 and 6 into cluster 5.

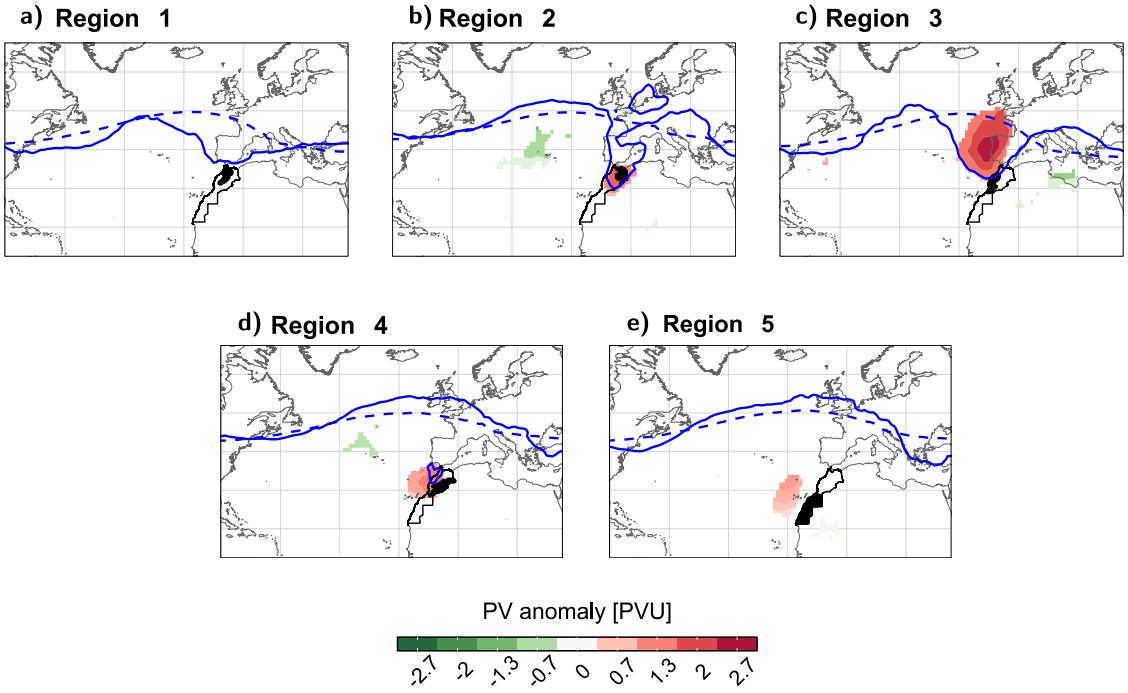

Fig. A.3. PV anomalies at the 330 K isentropic surface (shaded), climatological 2-PVU contour (dashed line), and 2-PVU contour averaged over extreme events in the area of interest.

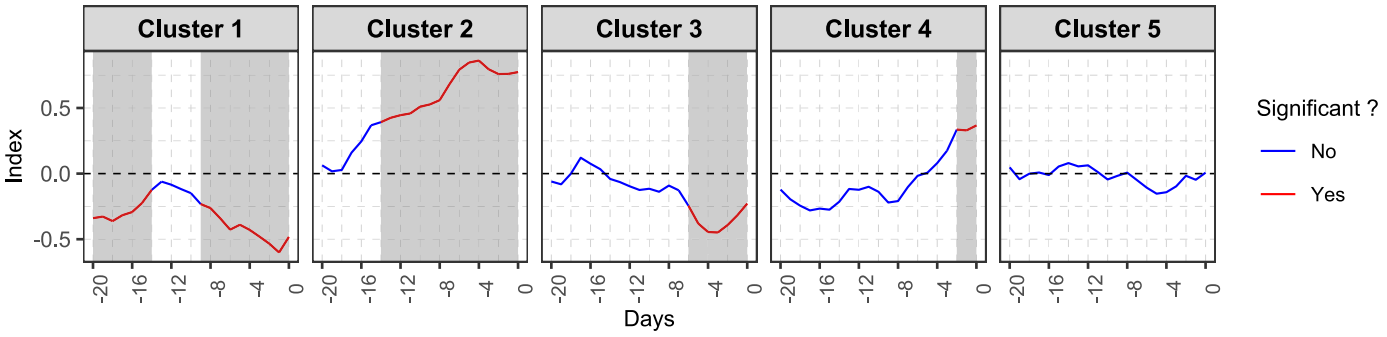

Fig. A.4. Average NAO index during the 20 days preceding EPEs in each region. The statistical significance of the index is evaluated using Algorithm B.2.

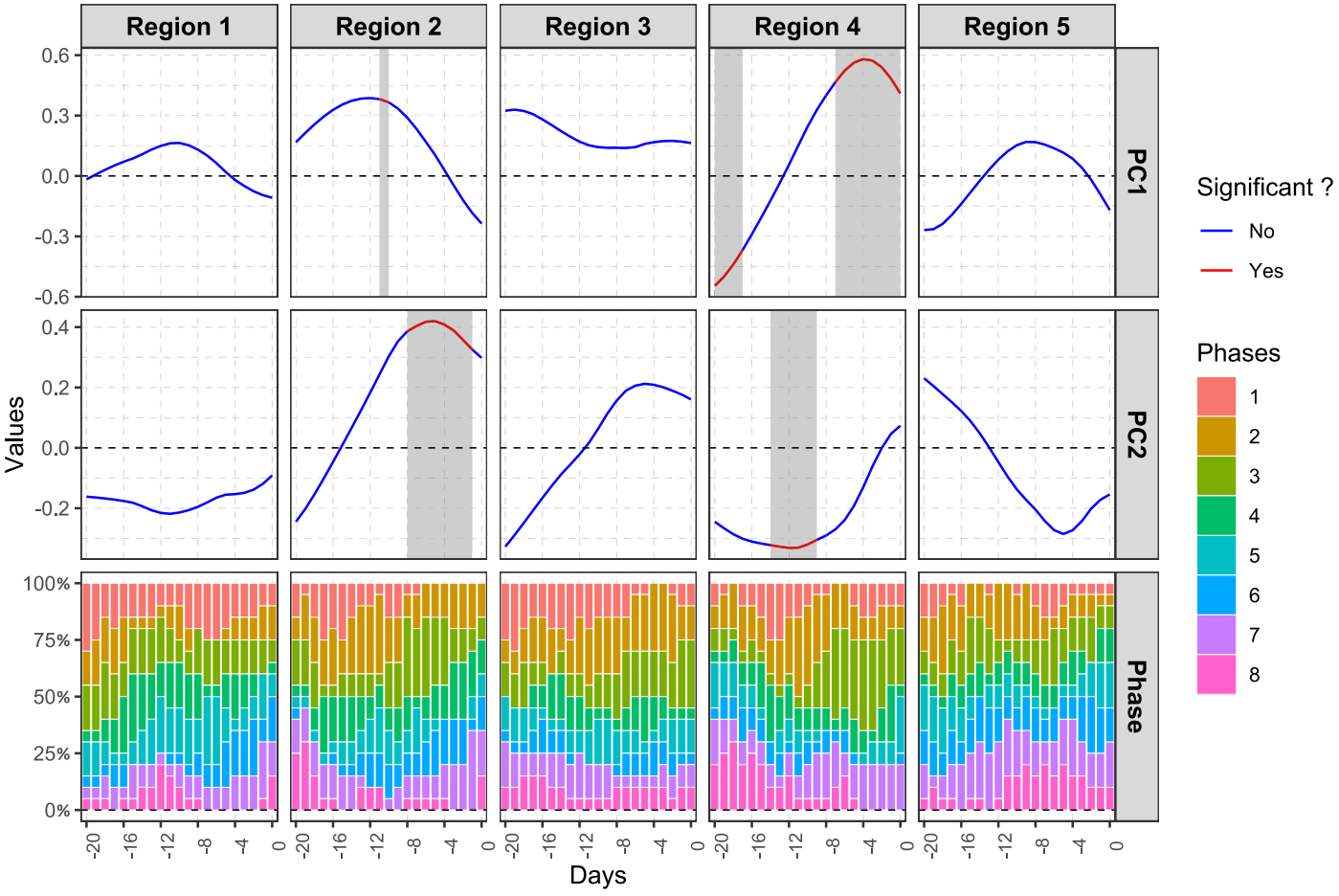

Fig. A.5. Average amplitudes, PC1 and PC2, and phases of MJO principal components (OMI index) during each of the 20 days leading up EPEs in each region (Fig. 2). The statistical significance of the index is evaluated using Algorithm B.2. The phases of the OMI (OLR-based MJO index) are calculated by considering $CP1 = OMI(CP2)$ and $CP2 = -OMI(CP1)$, in order to obtain phases comparable to those of the RMM (Real-time Multivariate MJO) index, for further details see Kiladis et al. (2014).

Appendix B. Algorithms

Algorithm B.1 : Probability of co-occurrence of extreme precipitation events

Data preparation : let
X_i = Daily precipitation time series at grid point i
threshold = 99th percentile of wet days ($X_i > 1 mm/day$)

Algorithm :

for grid point i from the study area **do** ▷ Computing extreme precipitation

$$\tilde{X}_i = \begin{cases} 1 & if\ X_i > threshold \\ 0 & otherwise \end{cases}.$$

end for

for C in Clusters **do**
  N_C = total number of grid points in cluster C
  for grid point i in C **do**
    $N_i = \sum \tilde{X}_i$ ▷ Number of days with extreme precipitation in i
    for grid point j fom the study area **do**

$$CoP(i,j) = \frac{\sum_{e=1}^{N_i} Occur_{ie}(j)}{N_i}, \text{ with } i \neq j.$$

    end for
  end for

$$CoP_C(j) = \frac{\sum_i CoP(i,j)}{N_C - 1},$$

return : $CoP_C(j)$
end for

Related function :

$$Occur_{ie}(j) = \begin{cases} 1 & \text{if an extreme event occurs in } j \\ & \text{within 3 days before or} \\ & \text{after the extreme event } e \text{ occurs in i} \\ 0 & otherwise \end{cases}.$$

Algorithm B.2 : Anomaly significance test

Input :
RA ← Mean anomaly of the atmospheric variable ▷ RA for "Real anomaly"
Dates ← Extreme event dates

Output:
Mask of local non-significant anomalies.

Algorithm :

Set **D** as empty list ▷ Set of dates used to generate anomalies
for *date* in **Dates do**
    d ← *date* ± 10 days
    D ← $Concatenate(\mathbf{D}, \mathbf{d})$
end for

Set **GAs** as empty list ▷ GAs for "Generated Anomalies"
for i=1 to 2000 **do**
    dates ← pull randomly 20 dates from **D**
    Set **GA** as empty list
    for *date* in **dates do**
        A ← the anomaly of the atmospheric variable on *date*
        GA ← $Concatenate(\mathbf{GA}, \mathbf{A})$
    end for
    GAs ← $Concatenate(\mathbf{GAs}, mean(\ \mathbf{GA}))$
end for

R ← rank of **RA** among **GAs**
calculate a *p-value* based on **R**
adjust the *p-value* using the *FDR* method
Mask ← *p-value* < 10% (anomaly mask)

return : Mask

References

Aide, T., Szönyi, M., Saidi, A.D., 2015. Morocco floods of 2014: what we can learn from Guelmim and Sidi Ifni. URL http://repo.floodalliance.net/jspui/handle/44111/1457.

Arnone, E., Pumo, D., Francipane, A., La Loggia, G., Noto, L.V., 2018. The role of urban growth, climate change, and their interplay in altering runoff extremes. Hydrol. Process. 32 (12), 1755–1770. http://dx.doi.org/10.1002/hyp.13141.

Balhane, S., Driouech, F., Chafki, O., Manzanas, R., Chehbouni, A., Moufouma-Okia, W., 2022. Changes in mean and extreme temperature and precipitation events from different weighted multi-model ensembles over the northern half of Morocco. Clim. Dynam. 58 (1), 389–404. http://dx.doi.org/10.1007/s00382-021-05910-w.

Batibeniz, F., Ashfaq, M., Önol, B., Turuncoglu, U.U., Mehmood, S., Evans, K.J., 2020. Identification of major moisture sources across the Mediterranean Basin. Clim. Dynam. 54 (9), 4109–4127. http://dx.doi.org/10.1007/s00382-020-05224-3.

Benabdelouahab, T., Gadouali, F., Boudhar, A., Lebrini, Y., Hadria, R., Salhi, A., 2020. Analysis and trends of rainfall amounts and extreme events in the Western Mediterranean region. Theor. Appl. Climatol. 141 (1), 309–320. http://dx.doi.org/10.1007/s00704-020-03205-4.

Bernard, E., Naveau, P., Vrac, M., Mestre, O., 2013. Clustering of maxima: Spatial dependencies among heavy rainfall in France. J. Clim. 26 (20), 7929–7937. http://dx.doi.org/10.1175/JCLI-D-12-00836.1.

Binder, H., Boettcher, M., Joos, H., Wernli, H., 2016. The role of warm conveyor belts for the intensification of extratropical cyclones in Northern Hemisphere winter. J. Atmos. Sci. 73 (10), 3997–4020. http://dx.doi.org/10.1175/JAS-D-15-0302.1.

Bracken, C., Rajagopalan, B., Alexander, M., Gangopadhyay, S., 2015. Spatial variability of seasonal extreme precipitation in the western United States. J. Geophys. Res.: Atmos. 120 (10), 4522–4533. http://dx.doi.org/10.1002/2015JD023205.

Browning, K.A., 1986. Conceptual models of precipitation systems. Weather Forecast. 1 (1), 23–41. http://dx.doi.org/10.1175/1520-0434(1986)001<0023:CMOPS>2.0.CO;2.

Cassou, C., 2008. Intraseasonal interaction between the Madden–Julian oscillation and the North Atlantic Oscillation. Nature 455 (7212), 523–527.

Cooley, D., Naveau, P., Poncet, P., 2006. Variograms for spatial max-stable random fields. In: Dependence in Probability and Statistics. Springer, pp. 373–390. http://dx.doi.org/10.1007/0-387-36062-X_17.

De Vries, A.J., 2021. A global climatological perspective on the importance of Rossby wave breaking and intense moisture transport for extreme precipitation events. Weather Climate Dyn. 2 (1), 129–161. http://dx.doi.org/10.5194/wcd-2-129-2021.

Doswell, C.A., Brooks, H.E., Maddox, R.A., 1996. Flash flood forecasting: An ingredients-based methodology. Weather Forecast. 11 (4), 560–581. http://dx.doi.org/10.1175/1520-0434(1996)011<0560:FFFAIB>2.0.CO;2.

Douglas, I., Alam, K., Maghenda, M., Mcdonnell, Y., McLean, L., Campbell, J., 2008. Unjust waters: climate change, flooding and the urban poor in Africa. Environ. Urbanization 20 (1), 187–205. http://dx.doi.org/10.1177/0956247808089156.

Driouech, F., Stafi, H., Khouakhi, A., Moutia, S., Badi, W., ElRhaz, K., Chehbouni, A., 2021. Recent observed country-wide climate trends in Morocco. Int. J. Climatol. 41, E855–E874. http://dx.doi.org/10.1002/joc.6734.

Eckhardt, S., Stohl, A., Wernli, H., James, P., Forster, C., Spichtinger, N., 2004. A 15-year climatology of warm conveyor belts. J. Clim. 17 (1), 218–237. http://dx.doi.org/10.1175/1520-0442(2004)017<0218:AYCOWC>2.0.CO;2.

El Hamly, M., Sebbari, R., 1998. Towards the seasonal prediction of Moroccan precipitation and its implications for water. VariabilitÉ Des Ressources En Eau En Afrique Au XXÈMe SiÈCle (252), 79.

Filahi, S., Tanarhte, M., Mouhir, L., El Morhit, M., Tramblay, Y., 2016. Trends in indices of daily temperature and precipitations extremes in Morocco. Theor. Appl. Climatol. 124 (3), 959–972. http://dx.doi.org/10.1007/s00704-015-1472-4.

Filahi, S., Tramblay, Y., Mouhir, L., Diaconescu, E.P., 2017. Projected changes in temperature and precipitation indices in Morocco from high-resolution regional climate models. Int. J. Climatol. 37 (14), 4846–4863. http://dx.doi.org/10.1002/joc.5127.

Fink, A.H., Knippertz, P., 2003. An extreme precipitation event in southern Morocco in spring 2002 and some hydrological implications. Weather 58 (10), 377–387. http://dx.doi.org/10.1256/wea.256.02.

Gadouali, F., Semane, N., Muñoz, Á., Messouli, M., 2020. On the link between the Madden-Julian oscillation, euro-mediterranean weather regimes, and Morocco Winter Rainfall. J. Geophys. Res.: Atmos. 125 (8), http://dx.doi.org/10.1029/2020JD032387, e2020JD032387.

Hersbach, H., Bell, B., Berrisford, P., Hirahara, S., Horányi, A., Muñoz-Sabater, J., Nicolas, J., Peubey, C., Radu, R., Schepers, D., et al., 2020. The ERA5 global reanalysis. Q. J. R. Meteorol. Soc. 146 (730), 1999–2049. http://dx.doi.org/10.1002/qj.3803.

IPCC, 2012. In: Field, C.B., Barros, V., Stocker, T., Qin, D., Dokken, D., Ebi, K., Mastrandrea, M., Mach, K., Plattner, G.-K., Allen, S., Tignor, M., Midgley, P. (Eds.), Managing the Risks of Extreme Events and Disasters To Advance Climate Change Adaptation. a Special Report of Working Groups I and II of the Intergovernmental Panel on Climate Change. Cambridge University Press, Cambridge, United Kingdom and New York, NY, USA, p. 582.

IPCC, 2022. In: Pörtner, H.-O., Roberts, D., Tignor, M., Poloczanska, E., Mintenbeck, K., a, A.A., Craig, M., Langsdorf, S., Löschke, S., Möller, V., Okem, A., Rama, B. (Eds.), Climate Change 2022: Impacts, Adaptation, and Vulnerability. Contribution of Working Group II to the Sixth Assessment Report of the Intergovernmental Panel on Climate Change. Cambridge University Press, (in press).

Jiang, X., Adames, Á.F., Kim, D., Maloney, E.D., Lin, H., Kim, H., Zhang, C., DeMott, C.A., Klingaman, N.P., 2020. Fifty years of research on the Madden-Julian Oscillation: Recent progress, challenges, and perspectives. J. Geophys. Res.: Atmos. 125 (17), http://dx.doi.org/10.1029/2019JD030911, e2019JD030911.

Jones, C., Waliser, D.E., Lau, K., Stern, W., 2004. Global occurrences of extreme precipitation and the Madden–Julian oscillation: Observations and predictability. J. Clim. 17 (23), 4575–4589. http://dx.doi.org/10.1175/3238.1.

Khomsi, K., Mahe, G., Tramblay, Y., Sinan, M., Snoussi, M., 2016. Regional impacts of global change: seasonal trends in extreme rainfall, run-off and temperature in two contrasting regions of Morocco. Nat. Hazards Earth Syst. Sci. 16 (5), 1079–1090. http://dx.doi.org/10.5194/nhess-16-1079-2016.

Khouakhi, A., Driouech, F., Slater, L., Waine, T., Chafki, O., Chehbouni, A., Raji, O., 2022. Atmospheric rivers and associated extreme rainfall over Morocco. Int. J. Climatol. http://dx.doi.org/10.1002/joc.7676.

Kiladis, G.N., Dias, J., Straub, K.H., Wheeler, M.C., Tulich, S.N., Kikuchi, K., Weickmann, K.M., Ventrice, M.J., 2014. A comparison of OLR and circulation-based indices for tracking the MJO. Mon. Weather Rev. 142 (5), 1697–1715. http://dx.doi.org/10.1175/MWR-D-13-00301.1.

Knippertz, P., Christoph, M., Speth, P., 2003. Long-term precipitation variability in Morocco and the link to the large-scale circulation in recent and future climates. Meteorol. Atmos. Phys. 83 (1), 67–88. http://dx.doi.org/10.1007/s00703-002-0561-y.

Knippertz, P., Martin, J.E., 2005. Tropical plumes and extreme precipitation in subtropical and tropical West Africa. Q. J. R. Meteorological Soc.: A J. Atmospheric Sci. Appl. Meteorology Phys. Oceanography 131 (610), 2337–2365. http://dx.doi.org/10.1256/qj.04.148.

Krichak, S.O., Breitgand, J.S., Gualdi, S., Feldstein, S.B., 2014. Teleconnection–extreme precipitation relationships over the Mediterranean region. Theor. Appl. Climatol. 117 (3), 679–692. http://dx.doi.org/10.1007/s00704-013-1036-4.

Lamb, P.J., Peppler, R.A., 1987. North Atlantic Oscillation: concept and an application. Bull. Am. Meteorol. Soc. 68 (10), 1218–1225. http://dx.doi.org/10.1175/1520-0477(1987)068<1218:NAOCAA>2.0.CO;2.

Leonard, K., Peter, J.R., 1990. Finding groups in data: an introduction to cluster analysis. Probability Math. Statist. Appl. Probability Statist..

Lin, Y.-L., Chiao, S., Wang, T.-A., Kaplan, M.L., Weglarz, R.P., 2001. Some common ingredients for heavy orographic rainfall. Weather Forecast. 16 (6), 633–660. http://dx.doi.org/10.1175/1520-0434(2001)016<0633:SCIFHO>2.0.CO;2.

Merino, A., Fernández-Vaquero, M., López, L., Fernández-González, S., Hermida, L., Sánchez, J.L., García-Ortega, E., Gascón, E., 2016. Large-scale patterns of daily precipitation extremes on the Iberian Peninsula. Int. J. Climatol. 36 (11), 3873–3891. http://dx.doi.org/10.1002/joc.4601.

Pfahl, S., Wernli, H., 2012. Quantifying the relevance of cyclones for precipitation extremes. J. Clim. 25 (19), 6770–6780. http://dx.doi.org/10.1175/JCLI-D-11-00705.1.

Rhodes, R., Shaffrey, L., Gray, S., 2015. Can reanalyses represent extreme precipitation over England and Wales? Q. J. R. Meteorol. Soc. 141 (689), 1114–1120. http://dx.doi.org/10.1002/qj.2418.

Rivoire, P., Martius, O., Naveau, P., 2021. A comparison of moderate and extreme ERA-5 daily precipitation with two observational data sets. Earth Space Sci. 8 (4), http://dx.doi.org/10.1029/2020EA001633, e2020EA001633.

Rohrer, M., Martius, O., Raible, C., Brönnimann, S., 2020. Sensitivity of blocks and cyclones in ERA5 to spatial resolution and definition. Geophys. Res. Lett. 47 (7), http://dx.doi.org/10.1029/2019GL085582, e2019GL085582.

Saidi, M.E., Daoudi, L., EL Hassane Arsmouk, M., Fniguire, F., Boukrim, S., 2010. Les crues de l'oued Ourika (Haut Atlas, Maroc): Événements extrêmes en contexte montagnard semi-aride.. ComunicaÇÕE GeolÓGicas 97 (1).

Satour, N., Raji, O., El Moçayd, N., Kacimi, I., Kassou, N., 2021. Spatialized flood resilience measurement in rapidly urbanized coastal areas with a complex semi-arid environment in northern Morocco. Nat. Hazards Earth Syst. Sci. 21 (3), 1101–1118. http://dx.doi.org/10.5194/nhess-21-1101-2021, URL https://nhess.copernicus.org/articles/21/1101/2021/.

Saunders, K., Stephenson, A., Karoly, D., 2021. A regionalisation approach for rainfall based on extremal dependence. Extremes 24 (2), 215–240. http://dx.doi.org/10.1007/s10687-020-00395-y.

Scaife, A.A., Folland, C.K., Alexander, L.V., Moberg, A., Knight, J.R., 2008. European climate extremes and the North Atlantic Oscillation. J. Clim. 21 (1), 72–83, URL http://www.jstor.org/stable/26260129.

Schreck III, C.J., 2021. Global survey of the MJO and extreme precipitation. Geophys. Res. Lett. 48 (19), http://dx.doi.org/10.1029/2021GL094691, e2021GL094691.

Theilen-Willige, B., Charif, A., El Ouahidi, A., Chaibi, M., Ougougdal, M.A., Ait-Malek, H., 2015. Flash floods in the Guelmim area/Southwest Morocco-use of remote sensing and GIS-tools for the detection of flooding-prone areas. Geosciences 5 (2), 203–221. http://dx.doi.org/10.3390/geosciences5020203.

Tramblay, Y., Badi, W., Driouech, F., El Adlouni, S., Neppel, L., Servat, E., 2012. Climate change impacts on extreme precipitation in Morocco . Glob. Planet. Change 82, 104–114. http://dx.doi.org/10.1016/j.gloplacha.2011.12.002.

Tramblay, Y., El Adlouni, S., Servat, E., 2013. Trends and variability in extreme precipitation indices over Maghreb countries. Nat. Hazards Earth Syst. Sci. 13 (12), 3235–3248. http://dx.doi.org/10.5194/nhess-13-3235-2013.

Tramblay, Y., Somot, S., 2018. Future evolution of extreme precipitation in the Mediterranean. Clim. Change 151 (2), 289–302. http://dx.doi.org/10.1007/s10584-018-2300-5.

Tuel, A., 2020. Precipitation Variability and Change Over Morocco and the Mediterranean (Ph.D. thesis). Massachusetts Institute of Technology, p. 287, URL https://hdl.handle.net/1721.1/129036.

Tuel, A., Eltahir, E.A., 2018. Seasonal precipitation forecast over Morocco. Water Resour. Res. 54 (11), 9118–9130. http://dx.doi.org/10.1029/2018WR022984.

Tuel, A., Kang, S., Eltahir, E.A., 2021. Seasonal precipitation forecast over Morocco. Clim. Dynam. 56, 985–1001. http://dx.doi.org/10.1007/s00382-020-05516-8.

Tuel, A., Martius, O., 2022. The influence of modes of climate variability on the sub-seasonal temporal clustering of extreme precipitation. Iscience 25 (3), 103855. http://dx.doi.org/10.1016/j.isci.2022.103855.

Tuel, A., Moçayd, N.E., 2023. Evaluating extreme precipitation in gridded datasets with a novel station database in Morocco. 10.22541%2Fessoar.167525285.54960295%2Fv1.

Ward, M.N., Lamb, P.J., Portis, D.H., Hamly, M.E., Sebbari, R., 1999. Climate variability in northern Africa: Understanding droughts in the Sahel and the Maghreb. In: Beyond El NiÑO. Springer, pp. 119–140. http://dx.doi.org/10.1007/978-3-642-58369-8_6.

Weibull, W., 1939. A Statistical Theory of Strength of Materials. IVB-Handl..

Westra, S., Alexander, L.V., Zwiers, F.W., 2013. Global increasing trends in annual maximum daily precipitation. J. Clim. 26 (11), 3904–3918. http://dx.doi.org/10.1175/JCLI-D-12-00502.1.

Wilks, D., 2016. "The stippling shows statistically significant grid points": How research results are routinely overstated and overinterpreted, and what to do about it. Bull. Am. Meteorol. Soc. 97 (12), 2263–2273. http://dx.doi.org/10.1175/BAMS-D-15-00267.1.